UC San Diego
UC San Diego Previously Published Works

Title

A Commensal Dipeptidyl Aminopeptidase with Specificity for N-Terminal Glycine Degrades Human-Produced Antimicrobial Peptides in Vitro

Permalink

https://escholarship.org/uc/item/210855j3

Journal

ACS Chemical Biology, 13(9)

ISSN

1554-8929

Authors

Xu, Janice H
Jiang, Zhenze
Solania, Angelo
et al.

Publication Date

2018-09-21

DOI

10.1021/acschembio.8b00420

Peer reviewed

A Commensal Dipeptidyl Aminopeptidase with Specificity for N-terminal Glycine Degrades Human-produced Antimicrobial Peptides *In Vitro*

Janice H. Xu[1,‡], **Zhenze Jiang**[2,‡], **Angelo Solania**[1], **Sandip Chatterjee**[1], **Brian M. Suzuki**[2], **Christopher B. Lietz**[2], **Vivian Hook**[2], **Anthony J. O'Donoghue**[2,*], **Dennis W. Wolan**[1,*]

[1]Department of Molecular Medicine, The Scripps Research Institute, 10550 North Torrey Pines Road, La Jolla, CA 92037

[2]Skaggs School of Pharmacy and Pharmaceutical Sciences, University of California, San Diego, 9500 Gilman Drive, La Jolla, CA 92093

Abstract

Proteases within the C1B hydrolase family are encoded by many organisms. We subjected a putative C1B-like cysteine protease secreted by the human gut commensal *Parabacteroidetes distasonis* to mass spectrometry-based substrate profiling to find preferred peptide substrates. The *P. distasonis* protease, we termed Pd_dinase, has a sequential di-aminopeptidase activity with strong specificity for N-terminal glycine residues. Using the substrate sequence information, we verified the importance of the P2 glycine residue with a panel of fluorogenic substrates and calculated k_{cat} and K_M for the dipeptide glycine-arginine-AMC. A potent and irreversible dipeptide inhibitor with a C-terminal acyloxymethyl ketone warhead, glycine-arginine-*AOMK*, was then synthesized and demonstrated that the Pd_dinase active site requires a free N-terminal amine for potent and rapid inhibition. We next determined the homohexameric Pd_dinase structure in complex with glycine-arginine-*AOMK* and uncovered unexpected active site features that govern the strict substrate preferences and differentiate this protease from members of the C1B and broader papain-like C1 proteases. We finally showed that Pd_dinase hydrolyzes several human antimicrobial peptides and therefore posit that this *P. distasonis* enzyme may be secreted into the extracellular milieu to assist in gut colonization by inactivation of host antimicrobial peptides.

Keywords

C1B protease; P. distasonis; commensal bacteria; antimicrobial peptide; diaminopeptidase

---

Efforts to structurally define new protein folds and assign potential function to uncharacterized proteins were spearheaded by high-throughput Protein Structure Initiative Centers over the last 15 years and several of these centers focused on the elucidation of proteins from commensal microbiome-associated bacteria.[1–4] One such structure (PDB ID: 3PW3) determined by the Joint Center for Structural Genomics (JCSG) was of an uncharacterized protein (Uniprot ID: A6LE66) from the gut commensal organism *Parabacteroidetes distasonis*. This bacterial species has been implicated in inflammatory bowel diseases (IBD); however, the role of *P. distasonis* in gut inflammation remains to be elucidated.[5, 6] Primary sequence analysis revealed that this protease, which we have called Pd_dinase, has limited homology to papain-like cysteine proteases. Yet, the apo Pd_dinase structure is strongly conserved in tertiary scaffold features with members of the bleomycin hydrolase (BLH) C1B (PF03051) family (Fig. S1A).

BLHs are cysteine hydrolases originally identified in humans for their ability to deamidate the anticancer glycopeptide bleomycin.[7–9] Broadly, members of the BLH family are responsible for the hydrolysis of homocysteine thiolactone and a range of other biological processes.[10, 11] For example, murine BLH degrades filaggrin,[12] and yeast BLH (Gal6) is a negative regulator of the galactose regulon[13] and has aminopeptidase activity.[14] In humans, BLH (hBLH) represents a potential drug discovery target to combat Alzheimer's disease,[15] as the protease processes amyloid precursor protein.[16] While the structures of Gal6 and hBLH demonstrate a strong conservation with cysteine proteases of the broader C1 papain-like family, the BLH subfamily is unique as these proteases form homo-hexamers and possibly homo-tetramers as reported for hBLH.[17] In its hexameric state, Gal6 and hBLH form a barrel-like structure akin to the proteasome with the active sites located within a central cavity (Fig. S1B). Limited accessibility to the cavity active sites are hypothesized to regulate proteolysis and control the spectrum of peptide/protein BLH substrates.[18, 19]

Proteases are essential for a wide variety of physiological reactions that are required for organismal survival. In the distal gut, proteases secreted by commensal bacteria are predicted to be involved in degradation of proteins and peptides for nutrient provision while also playing a role in evasion from host immune system recognition.[20–23] These proteases, along with other enzymatic functions can benefit the host via the breakdown of otherwise indigestible dietary constituents. Notwithstanding, secreted bacterial proteases are aberrantly increased in IBD and therefore, assigning their biological importance in both health and disease is of critical importance.[22–28]

Analysis of the primary sequence of A6LE66 produced by *P. distasonis*, suggested that Pd_dinase is highly conserved throughout the Bacterial Kingdom (Fig. S2). In addition, the protease contains a signal sequence that lacks a lipobox motif for post-translational lipid modification for insertion into bacterial membranes, and therefore is likely to be secreted into the distal gut. In this study, we sought to biochemically and structurally characterize the Pd_dinase protease. We confirmed that this protein is enzymatically active and found that it

preferentially removes dipeptides from the amino terminus of oligopeptides. An irreversible dipeptide inhibitor was synthesized based on the substrate specificity and was used for producing a co-crystal structure with Pd_dinase. This structure revealed several active site features that clearly distinguished Pd_dinase from other C1B family members and demonstrated why the protease preferentially removes dipeptides from the amino terminus of oligopeptides including the secreted human gut antimicrobial peptides, β-defensins and keratin-derived antimicrobial peptides. This in-depth biochemical and structural analysis of a C1B family protease may explain how commensal organisms colonize the human distal gut in the presence of host-secreted antimicrobials.

RESULTS AND DISCUSSION

Pd_dinase is a homo-hexamer

Pd_dinase was expressed with an N-terminal His_6-tag from E. coli and purified with a Ni-NTA affinity column followed by anion-exchange chromatography. Due to the significant structural commonalities between Pd_dinase and members of the BLH family, we speculated that the biologically relevant quaternary structure of Pd_dinase would likely be a multi-oligomer. We subjected our purified Pd_dinase to size exclusion chromatography coupled with multi-angle static light scattering (SEC-MALS) to accurately determine the oligomeric state and determined the mass of the complex to be 254 kD –/+ 1.1%. This mass corresponds to a homo-hexameric complex, as observed for yeast and human BLH (Fig. S3).

In vitro Pd_dinase substrate specificity

In order to biochemically characterize Pd_dinase, it was essential to uncover the substrate specificity of this enzyme. Pd_dinase was incubated with an equimolar mixture of 228 tetradecapeptides and the resulting cleavage products were evaluated by liquid chromatography coupled with tandem mass spectrometry (LC-MS/MS). This approach, termed multiplex substrate profiling by mass spectrometry (MSP-MS), has previously been used by our group to generate substrate specificity information for cysteine,[29] serine,[30] and threonine[31] proteases. Pd_dinase preferentially removed dipeptides from the amino terminus resulting in the formation of dodecapeptides (Fig. 1A). Many of these new cleavage products were subsequently degraded to decapeptides and then to octapeptides over time. For example, one such sequence among the 228 peptides, substrate GIQSTYFHDLNPYL, is hydrolyzed to FHDLNPYL by sequential removal of the dipeptides GI, QS and TY from the amino terminus (Fig. 1B).

We next generated a substrate specificity profile of the 70 cleavage sites detected between the 2nd and 3rd amino acids of the oligopeptides and determined that Pd_dinase has a strong preference for amino terminal Gly (*p*-value = 0.01), which corresponds to the P2 position (Fig. 1C). In addition, peptides containing small amino acids on the N-terminal, such as Ala, Ser and Thr, were frequently cleaved; however, peptides containing large hydrophobic or negatively charged amino acids at P2, such as Trp, Arg, Glu and Asp were unfavored (Fig. 1, Fig. S4).

Although this enzyme is clearly a di-aminopeptidase, two of the peptides in the library were hydrolyzed between the 3rd - 4th amino acids, indicating that Pd_dinase may have minor mono- or tri-aminopeptidase activity (Fig. 1A). Therefore, we utilized a selection of fluorescent substrates of increasing length to quantitatively compare the specificity of different aminopeptidases. Each substrate consisted of Arg linked to a cleavable aminomethylcoumarin (AMC) molecule as this amino acid is commonly used to assay C1B hydrolases.[11, 32] We predicted that Pd_dinase would preferentially cleave Gly-Arg-AMC relative to Arg-AMC or the N-terminally capped, glutamyl-Gly-Arg-AMC (Glt-Gly-Arg-AMC). As controls, we assayed the same set of substrates with human aminopeptidase B and bovine trypsin. Both enzymes have a preference for Arg in the P1 position; however, trypsin is an endopeptidase and aminopeptidase B cleaves single amino acids from the N-terminus.[33] Our assays confirmed that Pd_dinase does not cleave Arg-AMC or Glt-Gly-Arg-AMC but rapidly hydrolyzes Gly-Arg-AMC with k_{cat} and K_M values of 1.25 ± 0.02 sec^{-1} and 25.6 ± 1.7 μM (Fig. 1D, Fig. S5). In contrast, aminopeptidase B only cleaved Arg-AMC while trypsin cleaved Glt-Gly-Arg-AMC 80-fold more rapidly than Gly-Arg-AMC and failed to hydrolyze Arg-AMC. Taken together, these studies show that Pd_dinase is a sequential di-aminopeptidase with an unusual preference for N-terminal Gly residues.

In order to investigate the structural features that define the P2-Gly specificity, we synthesized a dipeptide inhibitor consisting of acyloxymethyl ketone (AOMK) reactive warhead. The AOMK warhead strongly reacts with nucleophilic cysteine residues and we showed that Gly-Arg-AOMK irreversibly inactivates Pd_dinase with a K_i of 683 ± 36 nM and k_{inact} of $3.6 \times 10^{-4} \pm 1.0 \times 10^{-5}$ sec^{-1} (Fig. 2A, B). To confirm that inhibition was not due to the reactivity of the warhead, we synthesized AOMK inhibitors consisting of N-terminally acetylated (Ac) and propynylated (Prop) Arg residue in place of the Gly-Arg dipeptide. While 50 μM of Gly-Arg-AOMK completely inhibited 2 nM of Pd_dinase, the same concentration of Ac-Arg-AOMK and Prop-Arg-AOMK had no effect on activity (Fig. 2C). These studies clearly show that potency of the Gly-Arg-AOMK was due to selectivity in the S2 pocket for Gly.

Co-crystal structure of Pd_dinase in complex with NH$_2$-glycine-arginine-AOMK

We determined the x-ray crystal structure of Pd_dinase (residues 24–405) in complex with GR-AOMK to 2.62 Å resolution (PDB ID: 5WDL) (Table S1). Each individual Pd_dinase monomer consists of 12 β-strands and 13 α-helices (Fig. S6). The protease has a core antiparallel β-sheet comprised of 6 β-strands, extending through the center of the protease that is protected by 6 α-helices donated by residues from the N-terminus on one face and 5 α-helices on the opposing face (Fig. S6). This canonical α/β/α sandwich is conserved among the cysteine peptidases. Interestingly, Pd_dinase has a structural feature unique to known C1 protease structures in that the longest β-strand (β9, residues 340–350) kinks at Gly346 and results in the contribution of 2 separate anti-parallel β-sheets (Fig. S7). The six monomers form a barrel-like structure with a cavity of approximately 33 Å and 88 Å in diameter and length, respectively. The final R_{cryst} and R_{free} values were 0.171 and 0.212, respectively, with 99% of the residues residing in the most favored region of the Ramachandran plot (Table S1). Excluding loop 286–310 (discussed below), there are few conformational changes between the GR-AOMK complex and 3PW3 apo structure with an

average rmsd = 0.17 Å and a maximum displacement of 1.31 Å. Electron density was not visible for residues 290–310 for subunits A, B, C, and D, as they comprise a loop with direct exposure to a solvent channel. Only residues 305–310 in subunit E lacked density and is likely due to stabilization of the loop region via interactions with a crystal contact. Continuous main-chain density was observed for chain F throughout the extended loop of 290–310, as F was the only subunit that established direct contact with an adjacent subunit within the hexamer (residues 365–370 of B). There was no direct evidence as to why only subunit F adopts this specific 290–310 loop conformation relative to the other 5 subunits.

Four β-sheets (β–7,9,10,11) and three α-helices (α–1,3,7) form the active site and are highly conserved across the C1 papain-like peptidase family (Fig. S6). Likewise, the Pd_dinase active site consists of the cysteine-histidine dyad common to cysteine proteases with the catalytic Cys56 positioned over the N-terminus of α–1 that promotes the pK$_a$ perturbation of the side-chain thiol (Fig. 3A). The naïve electron density maps clearly outlined the entire Gly-Arg peptide within the Pd_dinase active site covalently attached to Cys56 (Fig. 3B). Aside from the covalent bond between Cys56 and the inhibitor, the most significant interactions between Pd_dinase active site residues and the dipeptide are primarily via hydrogen bonds to the P2 Gly residue. The P2 primary amine is highly coordinated with three potential hydrogen bond acceptors, including the carboxylate side chains of Asp237 and Asp338 and the main-chain carbonyl of Gly109 (Fig. 3C). Presence of aspartic acids in the active site strongly support why substrates containing like charges (*i.e.,* Asp and Glu) at the N-terminus are disfavored (Fig. 1C). Non-specific peptide backbone interactions make up the rest of the potential hydrogen bonds. The P2 carbonyl interacts with main-chain amide of Gly109 and the amide nitrogen of P1 hydrogen bonds with the main-chain carbonyl of Asp339. The ketone moiety of the AOMK inhibitor is within hydrogen bonding distance to the His340 side chain; however, the side chain is not optimally oriented to accommodate an interaction with the inhibitor ketone in any of the 6 active sites within the structure. The P1 Arg side chain does not directly contact the protein and is held in position via a water-mediated network to the Asp237 side-chain carboxylate and Ser106 side-chain hydroxyl (Fig. 3C). Our structural studies strongly support the substrate specificity data, including: 1) the P1 side chain does not confer any substrate specificity (Fig. 3C); 2) the active site can only bind two non-prime side amino acids from substrates; 3) the shallow S2 subsite that interacts with P2 preferentially accommodates short aliphatic (Gly, Ala) or hydrogen bond donating (Ser, Thr) side chains that could provide hydrogen bonds with the main-chain carbonyls of Asp338 and Asp339 (Fig. 3D); 4) the active site discriminates against substrates with N-terminal Asp and Glu due to electrostatic repulsion and Trp and Tyr because of steric clashes (Fig. 3D); and 5) significant interactions between the N-terminal amine of the P2 residue substrate and the active site show that biologically relevant substrates likely require a free N-terminal amine with no post-translational modifications, including acetylation or propynylation (Fig. 3C).

Analysis of the active site surface and corresponding electrostatic potential revealed some surprising structural features. In general, the Pd_dinase active site is highly electronegative and fairly non-descript in the region that indirectly positions the P1 residue (Fig. 3D). Conversely, the P2 Gly of GR-AOMK is positioned directly over an entrance to a narrow channel that connects the interior active site to the solvent-exposed exterior (Fig. 3D). The

channel measures approximately 10 Å and 5 Å in length and width, respectively, and is also negatively charged. The structure depicted additional structured water molecules within the channel in comparison to the bound structures and may have a role in the hydrolysis mechanism of the enzyme. We posit that this channel strongly discriminates against most amino acids except residues with small and positively or uncharged side chains, such as Gly. Thus, this structural feature of Pd_dinase is the predominant restriction that confines substrate recognition to the small aliphatic P2 residues observed in the MSP-MS results (Fig. 1). The P2 channel contains several ordered water molecules and likely supplies the solvent necessary for regenerating the free cysteine thiol upon release of the hydrolyzed products (Fig. 3D).

Comparison of the apo and bound Pd_dinase structures

The unbound active site of the apo structure coordinates a Zn^{2+} ion via residues Cys56 and His340 introduced by $ZnCl_2$ from the crystallization buffer (Fig. 4A). When added in excess, Zn^{2+} inhibits substrate turnover and is likely caused by coordination to the Cys56 and His340 as well as the side-chain carboxylate oxygens of D298 from an adjacent subunit (Fig. 4A, Fig. S8). The bound Zn^{2+} locks loop 290–310 into an orientation whereby the tip of the loop (residues 296–303) occludes the neighboring active site pocket. The loop residues 290–310 are missing electron density in the GR-AOMK co-complex structure and suggest that the Zn^{2+} and loop are expelled upon active site binding (Fig. 4B). One monomer (F) in our GR-AOMK co-complex structure has density for residues 290–310 and superposition with the apo structure shows the loop moves approximately 30 Å upon active site binding and interacts with the same adjacent subunit within the hexamer (residues 365–370 of B) via a hydrogen bond between the main-chain carbonyl of Ala300 and the side-chain amide of Asn366 (Fig. 4B). Interestingly, the loop 290–310 conformation when upon occupation of the active site by substrate or inhibitor forms a small pore approximately 26 Å in width and 15 Å in height with primarily electronegative surface (Fig. 4C).

This unique conformational rearrangement revealed by the superposition of the apo and co-crystal structures likely has relevance to the biophysical mechanism of the protease. The flexible loop (residues 290–310) coordinated within an adjacent subunit's active site via a Zn^{2+} ion in the apo structure is expelled upon binding substrate or inhibitor and forms an electronegative pore (Fig. 4C). Such loop rearrangements have been observed in HIV-1 protease[34] and Crk signaling protein[35] that serve as a funnel for substrate binding and as a self-inhibitory mechanism, respectively. The conformational changes observed in these proteins are conferred by either Gly flexibility or Pro isomerization at a specified hinge region. Consistent with the other proteins, the flexible loop of Pd_dinase is flanked by Pro286, Pro316, and Pro318 on either side of the loop. We hypothesize that isomerization of one or more of the proline residues are likely to the shift between the open and closed conformation and these rearrangements could serve as a regulatory mechanism or may influence substrate recognition. Importantly, the much wider central channel formed by the homo-hexamers lacks any specific structural features or electrostatic charges that would help guide substrates to the active sites.

Comparisons to C1 papain-like structures

Dali structure similarity searches with Pd_dinase:GR-AOMK identified a list of papain-like cysteine proteases and endopeptidases despite little to no sequence homology. As expected, proteins with similar structural features include the C1B proteases hBLH (1CB5, Z = 32.9, rmsd = 3.1 Å, 321/453 residues),[11] Gal6 (1A6R, Z = 31.9, rmsd = 3.1 Å, 324/459 residues), [14] as well as *Lactobacillus rhamnosus* PepW (4K7C, Z = 34.0, rmsd = 2.9 Å, 322/446 residues). The structural similarities extend to include other members of the broader C1 papain-like proteases, such as *Clostridioides difficile* Cwp84 (4D5A, Z = 18.2, rmsd = 2.9 Å, 207/406 residues),[36] *Dionaea muscipula* dionain-1 (5A24, Z = 17.8, rmsd = 2.8 Å, 197/222 residues),[37] and EP-B2 (2FO5, Z = 17.6, rmsd = 2.8 Å, 194/224 residues)[38] (Fig. S9). Like most papain-like proteases, Pd_dinase prefers hydrophobic amino acids in the P2 position, but unlike the papain-like proteases, Pd_dinase strongly prefers Gly at the P2 position[39] and has no P1 specificity. In addition to different substrate specificity, Pd_dinase also forms an oligomer, which is unique to the C1B family. The most distinguishing feature that separates Pd_dinase from the rest of the aforementioned proteases is its unique substrate specificity, binding pocket, and channel by the active site.

Of the papain superfamily, only members of the C1B BLH-like family are currently known to form biologically relevant oligomers. Despite the high structural conservation between the monomeric units of Pd_dinase and the BLHs, the oligomerization states vary between tetrameric and hexameric forms, as both Pd_dinase and Gal6 are hexameric (Fig. S1B). Human BLH appears to be tetrameric *in vitro*; however, crystal structures suggest the protein can exist as both a tetramer and hexamer.[17] Despite Gal6 and Pd_dinase existing as hexamers, significant differences are observed in both the shape and diameter of the central channel as well as the electrostatic surface potentials (Fig. 5A). The central channel of Gal6 is shorter and has a narrower opening with a length and diameter of 66 Å and 22 Å that expands to 45 Å in the protein interior, respectively (Fig. 5A, S1B). This narrow opening has been predicted to confer selectivity for partially unfolded protein substrates that are funneled into the active sites. The central channel of Gal6 is lined with 60 lysine residues and as a result has a strong positive electrostatic potential (Fig. 5B). This charge distribution suggested that the central channel was the site of nucleic acid binding, as mutation of 3 lysine residues to alanine at the entrance to the channel abolished the nucleic acid binding activity.[11, 13] The surface-exposed residues within the central cavity and the outer region of Pd_dinase are primarily negative (Fig. 5B), as seen with the central channel of hexameric hBLH, which correlates with hBLH inability to bind nucleic acid. Conversely, Gal6 is more positive, which is consistent with its ability to bind single stranded DNA and RNA.

Localization of the proteases are also different. Native Pd_dinase is expressed with a signal sequence and is thus predicted to be secreted into the host environment. The BLH family, instead, are largely localized in the cytoplasm. This further supports that despite similar structural features, the two proteases serve different biological functions.

Antimicrobial peptide cleavage by Pd_dinase

We posited that potential biologically relevant Pd_dinase substrates would have an increased frequency of Gly residues. Certain classes of antimicrobial peptides (AMPs) are rich in Gly

and represent a common theme for host defense across different organisms, including bacteria,[40] plants,[41] and humans.[42] These AMPs have been found to mainly target Gram⁻ bacteria through outer membrane pore formations and DNA interactions. One set of human-derived Gly-rich AMPs are the keratin-derived antimicrobial peptides (KAMPs). KAMPs represent peptide fragments, ranging from 10 to 36 residues that are shed from the C-terminal region of the constitutively expressed human keratin 6A of stratified epithelial cells. [43] KAMP-14 (a 14-mer fragment) is bactericidal against *Pseudomonas aeruginosa*, *E. coli*, *Streptococcus pyogenes*, and *Staphylococcus aureus*.[42, 44] We synthesized KAMP-14 (GGLSSVGGGSSTIK) and KAMP-13 (AIGGGLSSVGGGS) using standard solid-phase peptide synthesis and incubated these peptides with Pd_dinase. Using the same LC-MS/MS-based approach to detect cleavage of the peptide library (Fig. 1A), we found that KAMP-14 is degraded into a 12-mer peptide due to removal of the amino terminal Gly-Gly dipeptide. This product is further processed into a 10-mer peptide after extended incubation with Pd_dinase (Fig. 6A). KAMP-13 was degraded into an 11-mer peptide following removal of Ala-Ile; however, this processing was slow with only 15.5% ($p = 0.013$) of the substrate being degraded by 1200 min. The 11-mer cleavage product consisted of an amino terminal Gly residue and was therefore rapidly hydrolyzed to a 9-mer peptide (Fig. 6B). We next incubated Pd_dinase with human β-defensin 2 (hBD2), a potent AMP produced in human epithelial cells that is upregulated in patients with ulcerative colitis.[45] The amino acids in position 2 and 3 are identical to KAMP-13 however this substrate has the preferred amino terminal Gly residue. Therefore, hBD2 was hydrolyzed faster than KAMP-13 with 51.2% at the substrate degraded by 60 min (Fig. 6C). Further cleavage of hBD2 by Pd_dinase between Asp and Pro could not be evaluated in this assay because partial hydrolysis of this bond occurred even in the absence of enzyme. The Asp-Pro bond is acid-labile[47] and was likely hydrolyzed during the sample acidification step prior to LC-MS/MS. As a control, we also incubated Pd_dinase with human neutrophil peptide 3 (HNP3), a well-studied human AMP that participates in systemic innate immunity. We predicted that this would not be cleaved by Pd_dinase because in contains disfavored Asp residue at the amino terminus. After 4 hours incubation of Pd_dinase with this peptide we failed to find a cleavage product and there was no significant reduction of HNP3 (Fig. S10).

The cleavage of the three human AMPs, with important roles as antibacterial, antiviral, and antifungal agents, clearly demonstrate the potential of these peptides as biological substrates of secreted Pd_dinase as well as related homologs from other commensal bacteria. While human AMP LL-37 has been shown to be hydrolyzed by bacterial proteases from pathogenic bacteria, including *S. aureus*[48] and *Bacillus anthracis*,[49] this is the first example demonstrating how commensal organisms may evade human gut bactericidal activity for colonization. The breadth of AMPs susceptible to Pd_dinase hydrolysis is a subject for further study, as most characterized secreted AMPs are 10–50 amino acids in length[50] and Pd_dinase prefers unmodified N-terminal Gly residues.

Pd_dinase may have additional biological substrates that are rich in Gly residues, including plant material and peptidoglycan layers of other bacteria. For example, many plants introduced through diet produce Gly-rich proteins often localized in cell walls and vacuoles and represent potential Pd_dinase substrates as a nutritional source for both the microbiome constituents and host. Similarly, the peptidoglycan layer of certain bacteria may be a source

of Pd_dinase substrates, such as *S. aureus.* The *S. aureus* peptidoglycan is comprised of poly-Gly chains employed by sortase A (SpA) to covalently adhere proteins with a LPXT/G motif. Additional studies will determine the scope of Pd_dinase targets and role in survival of *P. distasonis.*

CONCLUSIONS

We report the biochemical and structural characterization of a cysteine protease containing a canonical N-terminal secretion signal derived from the gut commensal bacteria *P. distasonis.* This protease is highly conserved across commensal gut bacteria and arranges in a homohexamer with all six active sites directed along a central cavity akin to bleomycin hydrolase. Using MSP-MS, kinetics, and x-ray crystallography, we have determined that this protease acts as a di-aminopeptidase with preference for N-terminal glycine. We demonstrate that potential biologically relevant substrates include several glycine-rich human antimicrobial peptides that are readily degraded by the protease. Our studies provide new mechanistic insights into how commensal bacteria may colonize the distal gut and overcome the presence of host antimicrobial agents.

METHODS

Pd_dinase expression and purification

The Pd_dinase WT clone from *Parabacteroidetes distasonis* ATCC 8503 (Protein Accession: WP_005854242, Uniprot ID: A6LE66) consisted of residues 24–405 without the N-terminal secretion leader sequence (residues 1–23) and was kindly provided by JCSG. Pd_dinase is expressed as an N-terminal His$_6$-tag fusion in *E. coli* BL21DE3pLysS (Strategene) and purified from clarified cellular lysate using a Ni-NTA affinity column followed by anion-exchange chromatography (details in Supporting Information). Fractions corresponding to Pd_dinase were pooled and immediately stored at −80 °C.

Peptide digestion assays

2 nM of Pd_dinase was incubated in triplicate with a mixture of 228 synthetic tetradecapeptides (0.5 μM each) in D-PBS with 2 mM DTT, and 10% of the reaction mixture was removed after 5, 15, 60, 240 and 1200 min of incubation. The activity was quenched with 6.4 M guanidine hydrochloride (GuHCl). A control reaction consisted of Pd_dinase treated with GuHCl prior to peptide exposure. 10 nM of Pd_dinase was incubated in triplicate with 5 μM of each antimicrobial peptide for 5, 15, 60, 240 and 1200 min and 10% of the reaction volume quenched with 6.4 M urea. A control reaction consisted of Pd_dinase treated with urea prior to peptide exposure. hBD2 and HNP3 was incubated with 5 mM DTT for 45 min at 55 °C. Afterwards free sulfhydryl groups were carbamidomethylated using 15 mM iodoacetamide for 30 min at room temperature in the dark. hBD2 and HNP3 were further digested with proteomic grade trypsin and GluC (Promega), respectively, for 20 h in 1:50 enzyme: protein ratio at 37 °C to generate detectable N-terminal fragments. All samples were stored at −80 °C prior to desalting and LC-MS/MS analysis (details in Supporting Information).

Fluorescent protease assays

Substrates containing aminomethylcoumarin (AMC) were purchased from Bachem and all assays were performed in D-PBS, 2 mM DTT. Pd_dinase (8 nM), human aminopeptidase B (2 nM) and bovine trypsin (100 nM) were assayed with 50 μM NH_2-arginine-AMC (Arg-AMC), NH_2-Gly-Arg-AMC (Gly-Arg-AMC), and Glutaryl-Gly-Arg-AMC for 30 min and the change in fluorescence monitored with excitation 360 nm and emission 460 nm using a Synergy HTX microplate reader (BioTek). Kinetic values, K_M and v_{max} were calculated over a range of 50 nM to 100 μM of Gly-Arg-AMC using 2 nM of Pd_dinase. For inhibitor screening, the reaction was initiated by adding 4 nM of Pd_dinase to a mixture of substrate and inhibitor such that the final enzyme, substrate and inhibitor concentrations were, 2 nM, 50 μM and 12.5 μM, respectively. Activity was monitored for 4 h. Inhibition values were calculated using 0.2 nM of enzyme, 300 μM GR-AMC and 0.5 nM to 2.048 μM of GR-AOMK (synthesis described in Supporting Information).

Data deposition

The atomic coordinates and structure factors have been deposited in the Protein Data Bank, www.wwpdb.org (PDB ID code 5WDL). Please see Supporting Information for crystallization and structure refinement.

Synthesis of keratin-derived antimicrobial peptides

KAMP-14 (NH_2-GGLSSVGGGSSTIK-COOH) and KAMP-13 (NH_2-AIGGGLSSVGGGS-COOH) were synthesized using standard FMOC-protected solid-phase peptide synthesis (details in Supporting Information). hBD2 was purchased from Peptides International, Inc.

Supplementary Material

Refer to Web version on PubMed Central for supplementary material.

ACKNOWLEDGMENT

ABBREVIATIONS

Ac	acetyl
AOMK	acyloxymethyl ketone
AMC	aminomethylcoumarin
AMP	antimicrobial peptide

BLH	bleomycin hydrolase
DTT	dithiothreitol
Gal6	yeast bleomycin hydrolase
hBD2	human β-defensin 2
HNP3	human neutrophil peptide 3
hBLH	human bleomycin hydrolase
IBD	inflammatory bowel disease
JCSG	Joint Center for Structural Genomics
KAMP	keratin-derived antimicrobial peptide
LC-MS/MS	liquid chromatography-tandem mass spectrometry
MSP-MS	multiplex substrate profiling by mass spectrometry
Prop	propynyl
SEC-MALS	size exclusion chromatography-multi-angle static light scattering
SpA	sortase A
WT	wildtype

REFERENCES

(1). Sheydina A, Eberhardt RY, Rigden DJ, Chang Y, Li Z, Zmasek CC, Axelrod HL, and Godzik A (2014) Structural genomics analysis of uncharacterized protein families overrepresented in human gut bacteria identifies a novel glycoside hydrolase. BMC Bioinformatics 15, 112. [PubMed: 24742328]

(2). Fleischman NM, Das D, Kumar A, Xu Q, Chiu HJ, Jaroszewski L, Knuth MW, Klock HE, Miller MD, Elsliger MA, Godzik A, Lesley SA, Deacon AM, Wilson IA, and Toney MD (2014) Molecular characterization of novel pyridoxal-5'-phosphate-dependent enzymes from the human microbiome. Protein Sci. 23, 1060–1076. [PubMed: 24888348]

(3). Bhowmik S, Jones DH, Chiu HP, Park IH, Chiu HJ, Axelrod HL, Farr CL, Tien HJ, Agarwalla S, and Lesley SA (2014) Structural and functional characterization of BaiA, an enzyme involved in secondary bile acid synthesis in human gut microbe. Proteins 82, 216–229. [PubMed: 23836456]

(4). Michalska K, Tan K, Li H, Hatzos-Skintges C, Bearden J, Babnigg G, and Joachimiak A (2013) GH1-family 6-P-β-glucosidases from human microbiome lactic acid bacteria. Acta Crystallogr. D Biol. Crystallogr 69, 451–463. [PubMed: 23519420]

(5). Kverka M, Zakostelska Z, Klimesova K, Sokol D, Hudcovic T, Hrncir T, Rossmann P, Mrazek J, Kopecny J, Verdu EF, and Tlaskalova-Hogenova H (2011) Oral administration of Parabacteroides distasonis antigens attenuates experimental murine colitis through modulation of immunity and microbiota composition. Clin. Exp. Immunol 163, 250–259. [PubMed: 21087444]

(6). Dziarski R, Park SY, Kashyap DR, Dowd SE, and Gupta D (2016) Pglyrp-regulated gut microflora Prevotella falsenii, Parabacteroides distasonis and Bacteroides eggerthii enhance and Alistipes finegoldii attenuates colitis in mice. PLoS One 11.

(7). Schwartz DR, Homanics GE, Hoyt DG, Klein E, Abernethy J, and Lazo JS (1999) The neutral cysteine protease bleomycin hydrolase is essential for epidermal integrity and bleomycin resistance. Proc. Natl. Acad. Sci. USA 96, 4680–4685. [PubMed: 10200322]

(8). Umezawa H, Takeuchi T, Hori S, Sawa T, and Ishizuka M (1972) Studies on the mechanism of antitumor effect of bleomycin of squamous cell carcinoma. J. Antibiot 25, 409–420. [PubMed: 4122312]

(9). Lazo JS, and Humphreys CJ (1983) Lack of metabolism as the biochemical basis of bleomycin-induced pulmonary toxicity. Proc. Natl. Acad. Sci. USA 80, 3064–3068. [PubMed: 6190169]

(10). Zimny J, Sikora M, Guranowski A, and Jakubowski H (2006) Protective mechanisms against homocysteine toxicity: the role of bleomycin hydrolase. J. Biol. Chem 281, 22485–22492. [PubMed: 16769724]

(11). O'Farrell PA, Gonzalez F, Zheng W, Johnston SA, and Joshua-Tor L (1999) Crystal structure of human bleomycin hydrolase, a self-compartmentalizing cysteine protease. Structure 7, 619–627. [PubMed: 10404591]

(12). Kamata Y, Taniguchi A, Yamamoto M, Nomura J, Ishihara K, Takahara H, Hibino T, and Takeda A (2009) Neutral cysteine protease bleomycin hydrolase is essential for the breakdown of deiminated filaggrin into amino acids. J. Biol. Chem 284, 12829–12836. [PubMed: 19286660]

(13). Zheng W, Xu HE, and Johnston SA (1997) The cysteine-peptidase bleomycin hydrolase is a member of the galactose regulon in yeast. J. Biol. Chem. 272, 30350–30355. [PubMed: 9374524]

(14). Zheng W, Johnston SA, and Joshua-Tor L (1998) The unusual active site of Gal6/bleomycin hydrolase can act as a carboxypeptidase, aminopeptidase, and peptide ligase. Cell 93, 103–109. [PubMed: 9546396]

(15). Papassotiropoulos A, Bagli M, Jessen F, Frahnert C, Rao ML, Maier W, and Heun R (2000) Confirmation of the association between bleomycin hydrolase genotype and Alzheimer's disease. Mol. Psychiatry 5, 213–215. [PubMed: 10822352]

(16). Lefterov IM, Koldamova RP, and Lazo JS (2000) Human bleomycin hydrolase regulates the secretion of amyloid precursor protein. FASEB J. 14, 1837–1847. [PubMed: 10973933]

(17). Koldamova RP, Lefterov IM, Gadjeva VG, and Lazo JS (1998) Essential binding and functional domains of human bleomycin hydrolase. Biochemistry 37, 2282–2290. [PubMed: 9485374]

(18). Lupas A, Flanagan JM, Tamura T, and Baumeister W (1997) Self-compartmentalizing proteases. Trends Biochem. Sci 22, 399–404. [PubMed: 9357316]

(19). Pickart CM, and Cohen RE (2004) Proteasomes and their kin: proteases in the machine age. Nat. Rev. Mol. Cell Biol 5, 177–187. [PubMed: 14990998]

(20). Gibson SA, McFarlan C, Hay S, and MacFarlane GT (1989) Significance of microflora in proteolysis in the colon. Appl. Environ. Microbiol 55, 679–683. [PubMed: 2648991]

(21). Macfarlane GT, Allison C, Gibson SA, and Cummings JH (1988) Contribution of the microflora to proteolysis in the human large intestine, J. Appl. Bacteriol 64, 37–46. [PubMed: 3127369]

(22). Carroll IM, and Maharshak N (2013) Enteric bacterial proteases in inflammatory bowel disease-pathophysiology and clinical implications. World J. Gastroenterol 19, 7531–7543. [PubMed: 24431894]

(23). Roka R, Rosztoczy A, Leveque M, Izbeki F, Nagy F, Molnar T, Lonovics J, Garcia-Villar R, Fioramonti J, Wittmann T, and Bueno L (2007) A pilot study of fecal serine-protease activity: a pathophysiologic factor in diarrhea-predominant irritable bowel syndrome. Clin. Gastroenterol. Hepatol 5, 550–555. [PubMed: 17336590]

(24). Carroll IM, Ringel-Kulka T, Ferrier L, Wu MC, Siddle JP, Bueno L, and Ringel Y (2013) Fecal protease activity is associated with compositional alterations in the intestinal microbiota. PLoS One 8, e78017. [PubMed: 24147109]

(25). Cenac N, Andrews CN, Holzhausen M, Chapman K, Cottrell G, Andrade-Gordon P, Steinhoff M, Barbara G, Beck P, Bunnett NW, Sharkey KA, Ferraz JG, Shaffer E, and Vergnolle N (2007) Role for protease activity in visceral pain in irritable bowel syndrome. J. Clin. Invest 117, 636–647. [PubMed: 17304351]

(26). Bustos D, Negri G, De Paula JA, Di Carlo M, Yapur V, Facente A, and De Paula A (1998) Colonic proteinases: increased activity in patients with ulcerative colitis. Medicina 58, 262–264. [PubMed: 9713093]

(27). Steck N, Mueller K, Schemann M, and Haller D (2012) Bacterial proteases in IBD and IBS. Gut 61, 1610–1618. [PubMed: 21900548]

(28). Vergnolle N (2016) Protease inhibition as new therapeutic strategy for GI diseases. Gut 65, 1215–1224. [PubMed: 27196587]

(29). Roncase EJ, Moon C, Chatterjee S, Gonzalez-Paez GE, Craik CS, O'Donoghue AJ, and Wolan DW (2017) Substrate profiling and high resolution co-complex crystal structure of a secreted C11 protease conserved across commensal bacteria. ACS Chem. Biol 12, 1556–1565. [PubMed: 28414448]

(30). Lentz CS, Ordonez AA, Kasperkiewicz P, La Greca F, O'Donoghue AJ, Schulze CJ, Powers JC, Craik CS, Drag M, Jain SK, and Bogyo M (2016) Design of selective substrates and activity-based probes for hydrolase important for pathogenesis 1 (HIP1) from Mycobacterium tuberculosis. ACS Infect. Dis 2, 807–815. [PubMed: 27739665]

(31). Li H, O'Donoghue AJ, van der Linden WA, Xie SC, Yoo E, Foe IT, Tilley L, Craik CS, da Fonseca PC, and Bogyo M (2016) Structure- and function-based design of Plasmodium-selective proteasome inhibitors. Nature 530, 233–236. [PubMed: 26863983]

(32). Bromme D, Rossi AB, Smeekens SP, Anderson DC, and Payan DG (1996) Human bleomycin hydrolase: molecular cloning, sequencing, functional expression, and enzymatic characterization. Biochemistry 35, 6706–6714. [PubMed: 8639621]

(33). Gainer H, Russell JT, and Loh YP (1984) An aminopeptidase activity in bovine pituitary secretory vesicles that cleaves the N-terminal arginine from β-lipotropin60–65. FEBS Lett. 175, 135–139. [PubMed: 6434344]

(34). Hornak V, Okur A, Rizzo RC, and Simmerling C (2006) HIV-1 protease flaps spontaneously open and reclose in molecular dynamics simulations. Proc. Natl. Acad. Sci. USA 103, 915–920. [PubMed: 16418268]

(35). Sarkar P, Saleh T, Tzeng SR, Birge RB, and Kalodimos CG (2011) Structural basis for regulation of the Crk signaling protein by a proline switch. Nat. Chem. Biol 7, 51–57. [PubMed: 21131971]

(36). Bradshaw WJ, Roberts AK, Shone CC, and Acharya KR (2015) Cwp84, a Clostridium difficile cysteine protease, exhibits conformational flexibility in the absence of its propeptide. Acta Crystallogr. F Struct. Biol. Comm 71, 295–303.

(37). Risor MW, Thomsen LR, Sanggaard KW, Nielsen TA, Thogersen IB, Lukassen MV, Rossen L, Garcia-Ferrer I, Guevara T, Scavenius C, Meinjohanns E, Gomis-Ruth FX, and Enghild JJ (2016) Enzymatic and structural characterization of the major endopeptidase in the venus flytrap digestion fluid. J. Biol. Chem 291, 2271–2287. [PubMed: 26627834]

(38). Bethune MT, Strop P, Tang YY, Sollid LM, and Khosla C (2006) Heterologous expression, purification, refolding, and structural-functional characterization of EP-B2, a self-activating barley cysteine endoprotease. Chem. Biol 13, 637–647. [PubMed: 16793521]

(39). Choe Y, Leonetti F, Greenbaum DC, Lecaille F, Bogyo M, Bromme D, Ellman JA, and Craik CS (2006) Substrate profiling of cysteine proteases using a combinatorial peptide library identifies functionally unique specificities. J. Biol. Chem 281, 12824–12832. [PubMed: 16520377]

(40). Bayer A, Freund S, and Jung G (1995) Post-translational heterocyclic backbone modifications in the 43-peptide antibiotic microcin B17. Structure elucidation and NMR study of a $^{13}C,^{15}N$-labelled gyrase inhibitor. Eur. J. Biochem 234, 414–426. [PubMed: 8536683]

(41). Park CJ, Park CB, Hong SS, Lee HS, Lee SY, and Kim SC (2000) Characterization and cDNA cloning of two glycine- and histidine-rich antimicrobial peptides from the roots of shepherd's purse, Capsella bursa-pastoris. Plant Mol. Biol 44, 187–197. [PubMed: 11117262]

(42). Tam C, Mun JJ, Evans DJ, and Fleiszig SM (2012) Cytokeratins mediate epithelial innate defense through their antimicrobial properties. J. Clin. Invest 122, 3665–3677. [PubMed: 23006328]

(43). Moll R, Divo M, and Langbein L (2008) The human keratins: biology and pathology. Histochem. Cell Biol 129, 705–733. [PubMed: 18461349]

(44). Lee JT, Wang G, Tam YT, and Tam C (2016) Membrane-active epithelial keratin 6A fragments (KAMPs) are unique human antimicrobial peptides with a non-αβ structure. Front. Microbiol 7, 1799. [PubMed: 27891122]

(45). Wehkamp J, Harder J, Weichenthal M, Mueller O, Herrlinger KR, Fellermann K, Schroeder JM, and Stange EF (2003) Inducible and constitutive beta-defensins are differentially expressed in Crohn's disease and ulcerative colitis, Inflamm. Bowel Dis 9, 215–223. [PubMed: 12902844]

(46). Hoover DM, Rajashankar KR, Blumenthal R, Puri A, Oppenheim JJ, Chertov O, and Lubkowski J (2000) The structure of human β-defensin-2 shows evidence of higher order oligomerization. J. Biol. Chem 275, 32911–32918. [PubMed: 10906336]

(47). Fung EN, Zambito F, Haulenbeek J, Piccoli SP, Zhang Y, DeSilva B, Arnold M, and Kozhich A (2014) Targeting an acid labile aspartyl-prolyl amide bond as a viable alternative to trypsin digestion to generate a surrogate peptide for LC-MS/MS analysis. Bioanalysis 6, 2985–2998. [PubMed: 25496253]

(48). Sieprawska-Lupa M, Mydel P, Krawczyk K, Wojcik K, Puklo M, Lupa B, Suder P, Silberring J, Silberring J, Reed M, Pohl J, Shafer W, McAleese F, Foster T, Travis J, and Potempa J (2004) Degradation of human antimicrobial peptide LL-37 by Staphylococcus aureus-derived proteinases. Antimicrob. Agents Chemother 48, 4673–4679. [PubMed: 15561843]

(49). Thwaite JE, Hibbs S, Titball RW, and Atkins TP (2006) Proteolytic degradation of human antimicrobial peptide LL-37 by Bacillus anthracis may contribute to virulence. Antimicrob. Agents Chemother 50, 2316–2322. [PubMed: 16801407]

(50). Guilhelmelli F, Vilela N, Albuquerque P, Derengowski LD, Silva-Pereira I, and Kyaw CM (2013) Antibiotic development challenges: the various mechanisms of action of antimicrobial peptides and of bacterial resistance. Front. Microbiol 4.
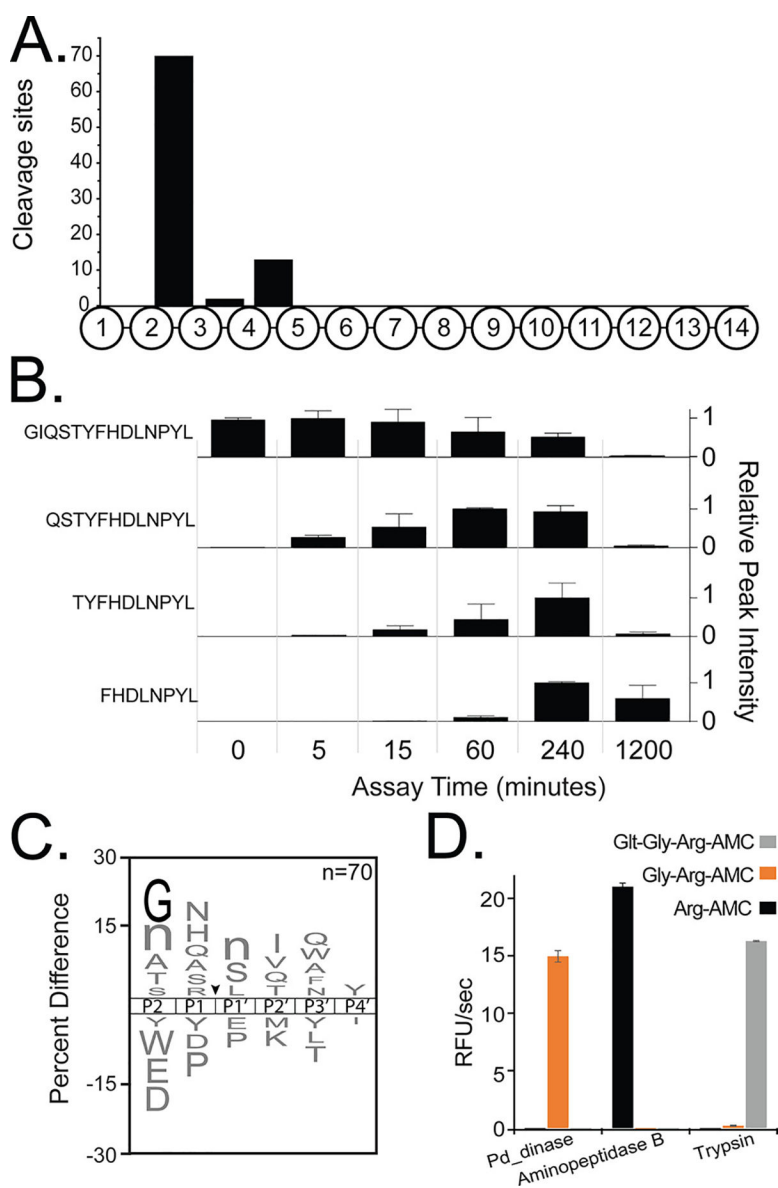
Fig. 1.
Pd_dinase is a sequential di-aminopeptidase. (A) Analysis of cleavage site location within the tetradecapeptide substrate library shows that hydrolysis after 5 minutes incubation generally occurs between the 2nd - 3rd, and 4th - 5th amino acids. (B) A sample peptide from the library showing time-dependent decrease in substrate with concomitant increase in degradation products. (C) An iceLogo plot illustrating the amino acids that are most frequently observed above X-axis and least frequently observed (below X-axis) at the P2 to P4′ positions that surround the cleavage site (black arrow). Glycine at P2 is highlighted in black, as it is the only residue that is significantly enriched (*p*-value < 0.01), lowercase 'n' corresponds to the non-natural amino acid, norleucine. (D) Evaluating Pd_dinase for mono-, di- and tri-aminopeptidase activity. Human aminopeptidase B and trypsin were used as control enzymes for the Arg-AMC and Glt-Gly-Arg-AMC substrates, respectively.
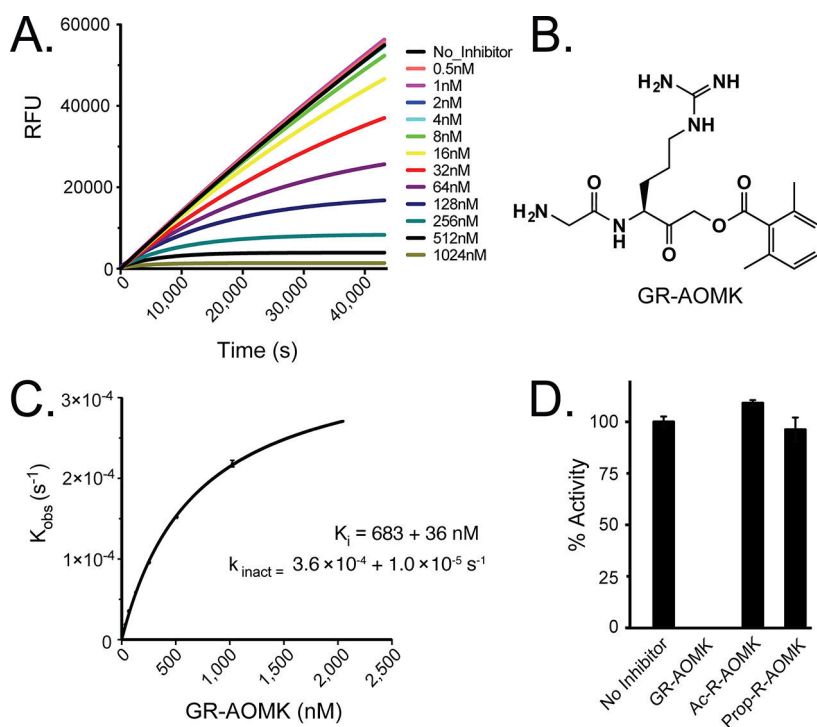
Fig. 2.
Pd_dinase is selectively inhibited by dipeptide inhibitors. (A) Incubation of Pd_dinase with 0.5 to 1024 nM of Gly-Arg-AOMK. (B) Chemical structure of Gly-Arg-AOMK. (C) Calculation of Ki and kinact. (D) Comparison of Pd_dinase activity in the presence of 50 μM of different peptide-AOMK inhibitors.
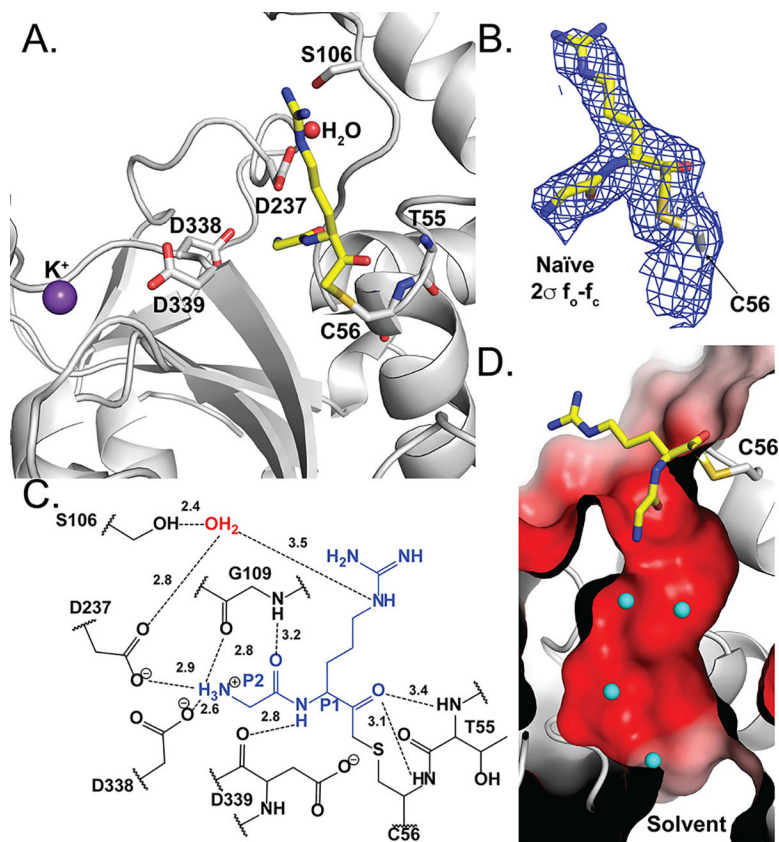
Fig. 3.
Pd_dinase in complex with the dipeptide inhibitor GR-AOMK determined by co-crystallization. (A) Cartoon representation of the residues and ordered water (red sphere) within the Pd_dinase:GR-AOMK structure. GR-AOMK (yellow carbon), covalently bound to the active Cys56, and active site residues (grey carbon) are shown as sticks (red oxygen, blue nitrogen, mustard sulfur). (B) The naïve f_o-f_c density map (blue) contoured at 2σ clearly indicated the orientation of the GR-AOMK dipeptide and covalent attachment to Cys56. (C) The hydrogen bonding network between GR-AOMK (blue), ordered water (red), and Pd_dinase active site residues (black) show that the majority of interactions with the inhibitor are to the N-terminal P2 Gly residue. (D) The surface electrostatic potential of the Pd_dinase active site consists of a highly electronegative channel that connects the solvent-exposed surface with the negatively charged active site, as shown with a cross-sectional representation. Ordered water molecules (cyan) are found throughout the channel. The electrostatic potential is colored: blue, positive potential (10 mV); white, neutral potential (0 mV); and red, negative potential (−10 mV).
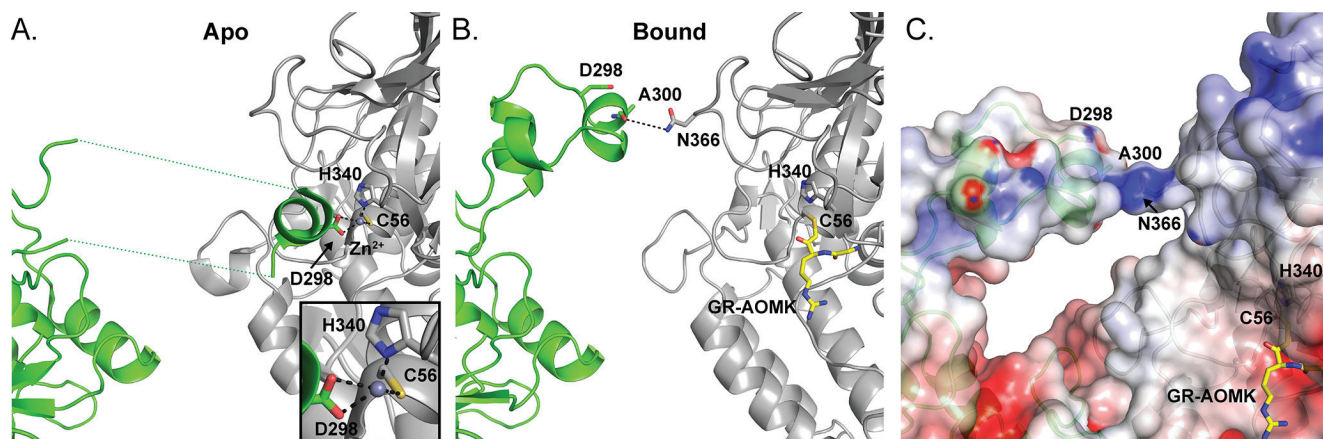
Fig. 4.
Loop 290–310 conformationally occludes neighboring active site with Zn^{2+} ion. Side-by-side comparison of the apo Pd_dinase (PDB ID: 3PW3, A) and Pd_dinase:GR-AOMK (B) structures demonstrate the flexibility of loop 290–310 from an active-site inhibited (apo, Zn^{2+} ion bound) conformation (see inset in A) to an active-site open (GR-AOMK-bound, B) with colors as in Fig. 3A. Potential hydrogen bonds are depicted as black dashes and residues 287–295 and 304–309 missing from the apo structure are represented by green dashed lines. (C) The active-site open conformation (GR-AOMK-bound) shows that the Ala300 main-chain carbonyl and the Asn366 side chain from the neighboring subunit hydrogen bond to form a pore. The surface electrostatic potential is as in Fig. 3D.
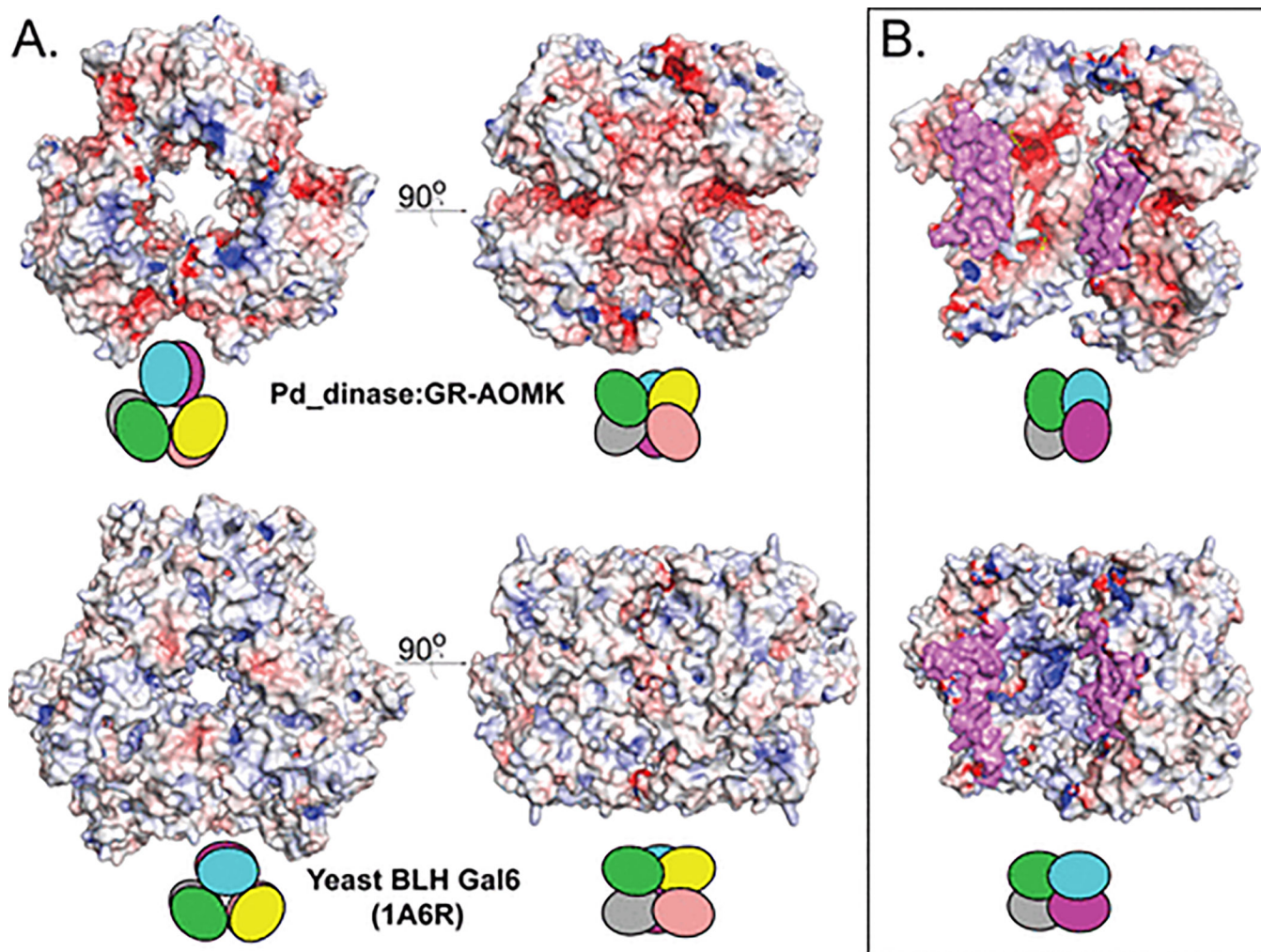
Fig. 5.
Comparison between Pd_dinase and yeast BLH homohexamers. (A) Surface representation and electrostatic potential of Pd_dinase (top) and yeast BLH Gal 6 (bottom) homohexamers accompanied by a schematic to illustrate the position of each chain. (B) Two chains are removed from the homohexamers to exhibit the electrostatic potential of the central channel. The interior of yeast BLH (bottom) is strongly positive while Pd_dinase (top) is slightly negative. The oligomer interface is colored magenta. The electrostatic surface potentials are calculated and colored according to Fig. 3.
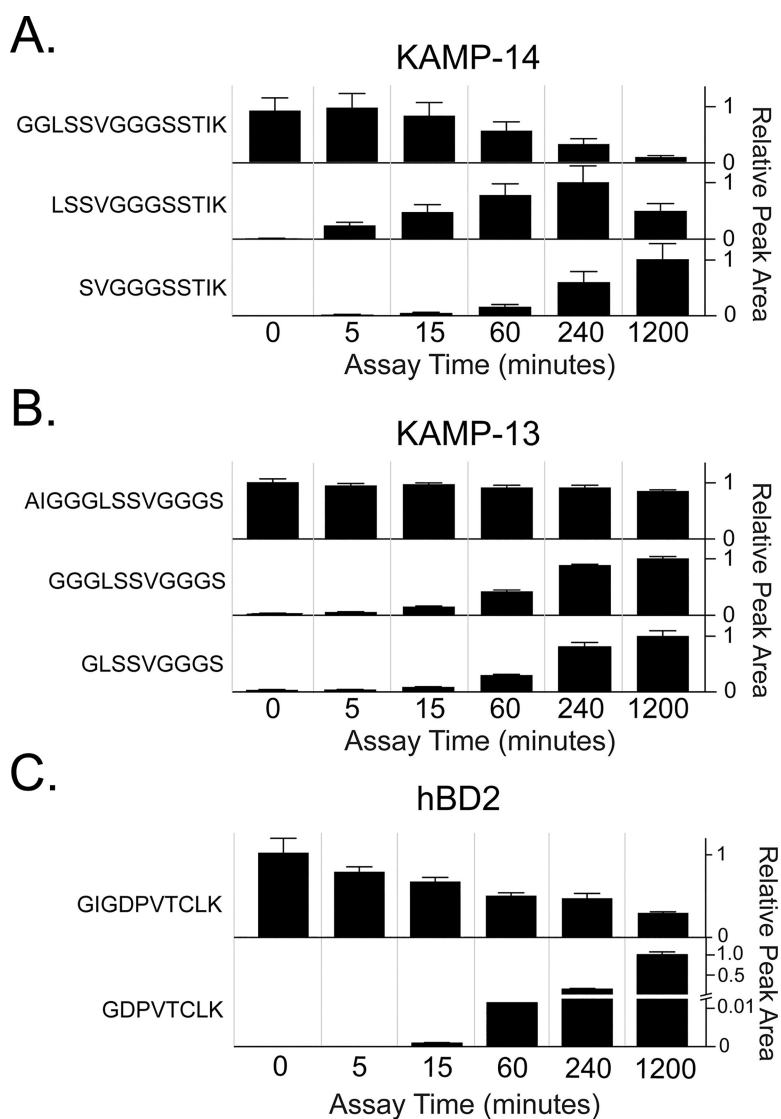
Fig. 6.
Hydrolysis of human antimicrobial peptides by Pd_dinase. (A) KAMP-14 is sequentially cleaved by Pd_dinase to a 12-mer and 10-mer. (B) Degradation of KAMP-13 to a 11-mer product is formed at a slower rate than KAMP-14 hydrolysis. The 11-mer product is efficiently cleaved further into a 9-mer peptide. (C) 51.2 of hBD2 is cleaved after 60 min incubation. Relative peak area is calculated from triplicate assays and normalized to the time interval with the highest mean peak area